JYX
JYVÄSKYLÄN YLIOPISTO
UNIVERSITY OF JYVÄSKYLÄ

This is a self-archived version of an original article. This version may differ from the original in pagination and typographic details.

Author(s): Dutta, Arpan; Alam, Khairul; Nuutinen, Tarmo; Hulkko, Eero; Karvinen, Petri; Kuittinen, Markku; Toppari, J. Jussi; Vartiainen, Erik M.

Title: Influence of Fano resonance on SERS enhancement in Fano-plasmonic oligomers

Year: 2019

Version: Published version

Copyright: © 2019 Optical Society of America under the terms of the OSA Open Access Publis

Rights:

Rights url:

Please cite the original version:

Dutta, A., Alam, K., Nuutinen, T., Hulkko, E., Karvinen, P., Kuittinen, M., Toppari, J. J., & Vartiainen, E. M. (2019). Influence of Fano resonance on SERS enhancement in Fano-plasmonic oligomers. Optics Express, 27(21), 30031-30043. https://doi.org/10.1364/OE.27.030031

Research Article | Vol. 27, No. 21 | 14 Oct 2019 | OPTICS EXPRESS 30031
Optics EXPRESS

Influence of Fano resonance on SERS enhancement in Fano-plasmonic oligomers

ARPAN DUTTA,[1,6] KHAIRUL ALAM,[2,8] TARMO NUUTINEN,[2,3,8] EERO HULKKO,[1,4] PETRI KARVINEN,[2] MARKKU KUITTINEN,[2] J. JUSSI TOPPARI,[1,7] AND ERIK M. VARTIAINEN[5]

[1]*Nanoscience Center and Department of Physics, University of Jyväskylä, FI-40014 University of Jyväskylä, Finland*
[2]*Institute of Photonics, University of Eastern Finland (UEF), FI-80101 Joensuu, Finland*
[3]*Department of Environmental and Biological Sciences, UEF, FI-80101 Joensuu, Finland*
[4]*Department of Electronics and Nanoengineering, Aalto University, FI-02150 Espoo, Finland*
[5]*School of Engineering Science, LUT University, FI-53851 Lappeenranta, Finland*
[6]*arpan.a.dutta@jyu.fi*
[7]*j.jussi.toppari@jyu.fi*
[8]*These authors contributed equally*

Abstract: Plasmonic oligomers can provide profound Fano resonance in their scattering responses. The sub-radiant mode of Fano resonance can result in significant near-field enhancement due to its light trapping capability into the so-called hotspots. Appearance of these highly localized hotspots at the excitation and/or Stokes wavelengths of the analytes makes such oligomers promising SERS active substrates. In this work, we numerically and experimentally investigate optical properties of two disk-type gold oligomers, which have different strength and origin of Fano resonance. Raman analysis of rhodamine 6G and adenine with the presence of the fabricated oligomers clearly indicates that an increment in the strength of Fano resonance can improve the Raman enhancement of an oligomer significantly. Therefore, by suitable engineering of Fano lineshape, one can achieve efficient SERS active substrates with spatially localized hotspots.

© 2018 Optical Society of America under the terms of the OSA Open Access Publishing Agreement

1. Introduction

Raman spectroscopy is nowadays a standard method for investigating the structural information of the materials [1,2]. Raman spectrum contains information about the vibrational and the rotational states in the molecular system of a probed material [3]. Extraction of such a chemical 'fingerprint' enables the use of Raman spectroscopy in different scientific and industrial applications ranging from ultra-violet (UV) to near-infrared (NIR) region [4,5]. Despite all acclaimed advantages of Raman spectroscopy, its real-life implementation is somewhat limited due to its low efficiency and sensitivity when compared, e.g., to fluorescence spectroscopy [6].

The observation of an intense Raman response at the presence of a silver electrode by Fleischmann and co-workers in 1974 [7], and the theoretical explanation of the phenomenon by Van Duyne et al. in 1977 [6], opened an efficient way to enhance the Raman signal with the help of subwavelength metallic structures [8-11]. That is, the presence of a plasmonic substrate leads to vastly enhanced Raman signal, i.e., Surface-Enhanced Raman Scattering (SERS) [12-14]. Advancement in nanofabrication technologies, specifically in electron-beam and focused-ion beam lithography, makes the realization of SERS active substrates with predefined sizes, shapes, and the material properties so accurate that SERS has become a popular method in bio-sensing [15-17], and in single molecule detection [18-21].

Suitable engineering of plasmonic resonances in complex photonic structures can optimize the enhancement of Raman response of a material. Generation of Fano resonance (FR) in a coupled plasmonic system is one way to do it [22]. Fano resonance is an asymmetric non-

#375061 https://doi.org/10.1364/OE.27.030031
Journal © 2019 Received 8 Aug 2019; revised 12 Sep 2019; accepted 13 Sep 2019; published 2 Oct 2019

Optics EXPRESS

Lorentzian resonance formed as an interference between a broad continuum state and a narrow discrete state [23-28]. It was first reported in 1935 when found in the absorption spectra of noble gases [23-27]. Even though FR had its implementation mainly in quantum systems in the past decades, it can also be generated profoundly in plasmonic oligomers [29-31].

Plasmonic oligomers are clusters of metallic nanoparticles (NP) where size, shape, and interparticle distance are specially arranged to obtain the desired optical response. Presence of multiple nanoparticles very close to each other induces interference and coupling between the localized surface plasmon resonances (LSPR) of individual NPs. Such hybridization of particle plasmon modes opens the possibility of having profound FR in the scattering or extinction profile of the system [30,31]. In a plasmonic oligomer, when the plasmon oscillations of all particles are in phase, they interfere constructively and the net dipole moment of the structure increases. Such collective mode provides a broad peak in the scattering spectrum that is often called as the super-radiant mode or bright mode. The dark mode or the sub-radiant mode is found as a dip in the scattering profile and is generated due to the destructive interference between the LSPR modes of individual particles when the plasmon oscillations are not in phase and the net dipole moment decreases [32-35]. The depth of the Fano dip indicates the strength of the coupling between LSPR modes of the nanoparticles and can be modulated by varying the gap between the particles [31]. When the gaps between the particles widen, the coupling between the plasmon modes of each particle reduces and the Fano dip starts to disappear. If the gap becomes very small, the coupling greatly enhances and the depth of the Fano dip almost reaches to the zero level, which is referred as the plasmon-induced transparency [36]. The spectral position of FR can be tuned by controlling the structural and chemical properties of the oligomer such as size, shape, thickness and material of the particles present in the oligomer while the gap between the particles defines the strength of the coupling [31,37].

The sub-radiant (or dark) mode in a Fano resonant plasmonic system can significantly enhance the near-field intensity within the nanostructure due to its non-radiative nature and capability to trap energy at the gaps between the particles [38]. The highest near-field intensity is always obtained near the Fano dip or Fano window [39], and consequently, Fano-plasmonic structures can provide large Raman enhancements when the FR is tuned with the excitation frequency and the targeted Stokes frequencies of the analytes [22]. Origin of FR in a plasmonic oligomer can be explained theoretically with the help of multiple approaches such as the coupled oscillator model [40-42], the subgroup decomposition of plasmonic resonances [35,43], the circuit model of Fano resonance [44], and the rigorous quantum electrodynamic formulation [45].

In this article, we report on the SERS activity of two disk-type gold oligomers, a trimer and a pentamer, which have profound FR in their scattering profile but with different origin and strength. The origin of FR in the pentamer is purely electric in nature [38,42,46-48], while FR in the trimer is generated due to the interaction between the electric and the magnetic plasmon modes [49-52]. The strength of FR, which can be identified by the depth of the Fano dip, is higher in the pentamer than in the trimer. The oligomers were numerically modelled using the finite element method (FEM) to tune their FR into the targeted Raman signals of two Raman active analytes, 1360 cm^{-1} for rhodamine 6G [53], and 734 cm^{-1} for adenine [54]. Optical characterization of the fabricated oligomers showed agreement with the simulated responses and ensured deeper Fano dip in the pentamer than in the trimer. Raman spectroscopy of rhodamine 6G and adenine with the presence of the oligomers showed higher SERS intensity in the case of the pentamer than with the trimer for both analytes. Our experimental findings show how the strength of FR, in terms of the depth of the Fano dip, directly influences the SERS activity of the oligomer when it is tuned with the targeted Raman region of the analytes. Such investigation on the dependence of SERS enhancement on the strength of FR in plasmonic oligomers having different Fano origin is not reported earlier for our knowledge.

Optics EXPRESS

2. Methods

2.1 Numerical simulations

Optical responses of the plasmonic oligomers were calculated and optimized numerically with FEM-based commercial software package (COMSOL Multiphysics version 5.1). In the computation, a single oligomer was placed on top of a glass substrate, and it was surrounded by air. The perfectly matched layers were used at all the boundaries of the 2 μm × 2 μm × 2 μm simulation space to prevent any reflections. The optical response of the oligomer, at the near– and far-field, for the normal incidence of light with electric field along the oligomer's main axis as illustrated in Fig. 1, was computed using the scattered-field formulation module of COMSOL [55]. The material model for gold was extracted from the measured optical constants recorded by Johnson and Christy [56]. The nondispersive refractive indices of air and glass (SiO_2) were considered as 1.0000 and 1.4585, respectively.

2.2 Fabrication

The plasmonic oligomers were fabricated using electron beam lithography and lift-off process. A 0.5 mm thick silicon (Si) wafer, with a 100 nm thick 'thermally grown' silicon dioxide (SiO_2) layer on it, was used as a substrate. A standard positive e-beam resist (AR-P 6200) was initially spin-coated on the substrate. The resist was patterned in an e-beam lithography system (Raith EBPG 5000+) according to the optimized design parameters obtained from the numerical simulations. Thermal evaporation method was used to deposit a uniform gold layer with a thickness of 20 nm on the patterned substrate, after which the resist was removed in a solvent resulting in gold structures on SiO_2. The schematics of the fabricated trimers and pentamers are shown in Fig. 1. The structures were organized as a square array on the substrate with a gap of 2 μm between each oligomer both in x and y directions to ensure prevention of any kind of coupling between them. Scanning electron microscope (SEM) imaging was used (SEMleo1550Gemini operated at an accelerated voltage of 5 kV) to determine the structures of the fabricated samples.

2.3 Optical characterization

Fabricated oligomers were characterized with a custom build optical setup where a white light source (Oriel 66182) was used to illuminate the array of gold trimers and pentamers. The light coming from the lamp was pseudo-collimated at best and two irises were used to align it. Rotatable Glan-Taylor polarizer was used to select the polarization of the excitation light. The scattering profiles of the oligomers were recorded by tracing the peak intensities of the reflected first diffraction order of the oligomer array at different angular positions by using a full 360° rotatable detection arrangement (F220SMA-A/ThorLabs, f = 10.9 mm, NA = 0.25). The angle-resolved scattering was collected with an optical fiber connected to a spectrometer (Jobin Yvon iHR320) equipped with a CCD camera (Jobin Yvon Symphony). More details about the optical setup can be found elsewhere [57-59].

2.4 Raman spectroscopy of analytes

Raman responses of rhodamine 6G and adenine for both kinds of oligomers were collected using a commercially available Raman setup (Renishaw inVia confocal Raman microscope) where a continuous-wave gas laser with an emission wavelength of 785 nm was used as an excitation source. A numerical objective (100X, NA = 0.85) was used to illuminate the sample for 30 s with 3.10 mW excitation power and to collect the Stokes-shifted signal. The correct polarization of the tightly focused excitation beam with 1 μm (approximated) spot size was maintained by rotating the sample stage. The analytes were deposited on the substrates with fabricated trimers and pentamers within a 10 μL water droplet and then incubated at room temperature under normal humidity for 5 minutes until the drop had dried. The initial

Optics EXPRESS

concentrations of the analytes in solution were 1 μM for rhodamine 6G (R6G) and 1 mM for adenine (Ade).

3. Results and discussion

Plasmonic oligomers were optimized using FEM-based simulations so that their FR would overlap with the targeted Raman signature zones of the analytes (1360 cm^{-1} for rhodamine 6G [53] and 734 cm^{-1} for adenine [54]) when excited with the wavelength of the Raman experiment (785 nm). The trimer, depicted in Fig. 1(a), contains a pair of identical disks having a radius of 50 nm along with a larger disk with a radius of 100 nm. The pentamer, presented in Fig. 1(b), contains a chain of three identical disks having a radius of 75 nm and two small identical disks with a radius of 62.5 nm on the top and the bottom of the central disk of the chain. The gap between the disks and the thickness (or height) of the disks are kept 20 nm in both oligomers to ensure that the difference between the strength of FR in those oligomers did not occur due to the difference in their interparticle distances and thicknesses. All geometric parameters related to the disks (i.e. interparticle gap, thickness and disk radius) had fabrication tolerances of ±5 nm obtained from the numerical simulations.

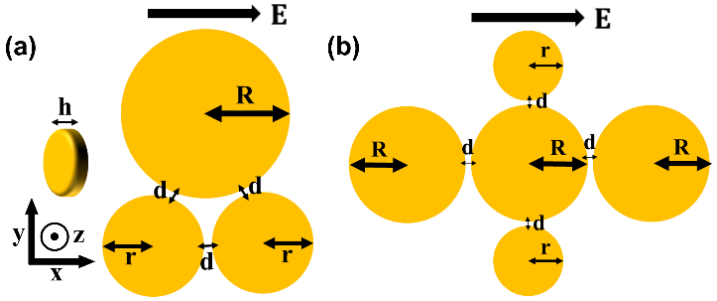

Fig. 1. (a) Optimized geometry for the trimer with R = 100±5 nm, r = 50±5 nm, d = 20±5 nm, h = 20±5 nm. (b) Optimized geometry for the pentamer with R = 75±5 nm, r = 62.5±5 nm, d = 20±5 nm, h = 20±5 nm. All geometric parameters related to the disks (i.e. interparticle gap, thickness and disk radius) had fabrication tolerances of ±5 nm obtained from the numerical simulations. The arrows on top of the structures show the polarization of the excitation.

The existence of FR and its overlap with the intended spectral regimes are clearly seen in the simulated scattering cross-sections of the oligomers, presented in Fig. 2(a) after normalized by their geometrical cross-sections. The strength of FR, in terms of the depth of the Fano dip, can be quantified by a parameter k, which defines the ratio between the scattering cross-sections (or scattering intensities) at the Fano dip ($S_{\text{Fano dip}}$) and at the Fano peak ($S_{\text{Fano peak}}$), i.e. $k = S_{\text{Fano dip}}/S_{\text{Fano peak}}$. The pentamer shows a lower value of k (k=0.21) than the trimer (k=0.43) in the simulated spectra and hence, provides higher depth in FR and stronger FR than the trimer. The spectral profiles of the total near-field intensity enhancement (NFIE) for the oligomers were calculated as $|E_{\text{loc}}/E_0|^2$ integrated over the illuminated surfaces of the oligomers (i.e. the top and sides of the disks), where E_{loc} and E_0 are the local and incident electric field amplitudes, respectively. The NFIE profiles, normalized by the geometrical surface area of the corresponding illuminated surfaces, are depicted in Fig. 2(b). They yield higher enhancement in the case of the pentamer than in the case of the trimer. The spectral position of the highest enhancement was found close to the Fano dip in the scattering spectra for both oligomers. Such spectral correlation between the scattering minima and the NFIE maxima is a general property of systems having FR [39], and has been reported earlier also for different kind of structures [22].

Optics EXPRESS

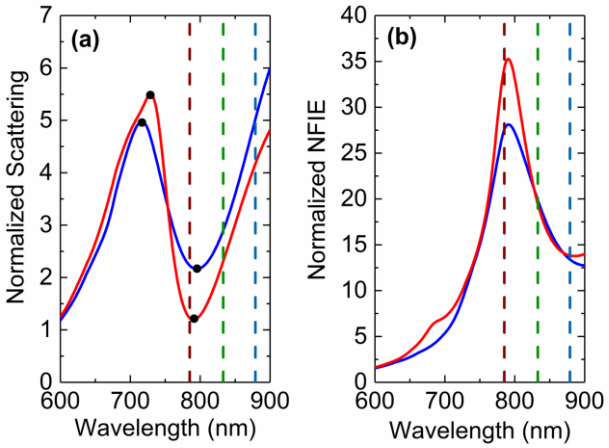

Fig. 2. (a) Simulated scattering cross-sections of the trimer (blue line) and the pentamer (red line). The black dots represent the position of the peak and the dip in the corresponding spectra used to calculate k. (b) Simulated NFIE of the trimer (blue line) and the pentamer (red line). The red, green and blue dashed lines in both diagrams represent, the excitation wavelength (785 nm), the targeted Raman line of adenine (734 cm^{-1} or 833 nm) and the targeted Raman line of rhodamine 6G (1360 cm^{-1} or 879 nm), respectively.

The near-field enhancement (NFE) maps $|E_{loc}/E_0|$ for the trimer and the pentamer, computed at a plane 1 nm above the top surfaces of the oligomers and presented in Fig. 3, show the spatial distribution of the NFE at the wavelengths of Fano dips and Fano peaks. The NFEs obtained at Fano dips (790 nm for the pentamer and 795 nm for the trimer) are higher than those of at Fano peaks (728 nm for the pentamer and 716 nm for the trimer) for both oligomers and their spatial distribution yields 'hotspots', i.e. confined regions with localized electromagnetic energy, at the gaps between the disks. In the trimer, the hotspots are found at the gap between the two small disks, showed in Fig. 3(a) and Fig. 3(b). In the pentamer, they situate at the gaps in the chain of the three identical disks, illustrated in Fig. 3(e) and Fig. 3(f), and they spatially overlap at both dip and peak wavelengths. The spatial locations of the hotspots at different wavelengths are not identical in general and are often distributed differently over the sample geometry [51]. Spatial overlap of the hotspots at multiple wavelengths is important for SERS applications since the electromagnetic enhancement factor (EEF) for SERS is defined as SERS EEF $= |E_{loc(excitation)}/E_0|^2 \times |E_{loc(Stokes)}/E_0|^2$ i.e. the product of the NFEs at the excitation and Stokes wavelengths [22]. Thus, spatially coinciding hotspots of these two wavelengths will yield the highest enhancement. The spatial distribution of the SERS EEFs (or SERS maps) for both oligomers at the targeted Raman signature zones of the analytes are reported in Fig. 3. From the figure we can see that the maximum SERS electromagnetic enhancement factors are about 3×10^6 for the trimer and 5×10^6 for the pentamer. Both of them are achieved for the 734 cm^{-1} Raman line of adenine.

Origin of FR in the trimer and the pentamer was investigated by computing the surface charge densities and the conduction current densities over the top surfaces of the disks. The surface charge density plots for the pentamer presented in Fig. 4 clearly show 'in-phase' plasmon oscillations in all disks at Fano peak (728 nm), shown in Fig. 4(a), but 'out of phase' oscillation in the central disk with respect to the other four disks at Fano dip (790 nm), shown in Fig. 4(b). This clearly explains generation of the broad super-radiant mode at 728 nm and the sub-radiant mode at 790 nm in the corresponding scattering profile. We can also infer that the nature of FR in the pentamer is purely electric since the interaction between the electric dipole moments causes the generation of FR [38,42,46-48].

Optics EXPRESS

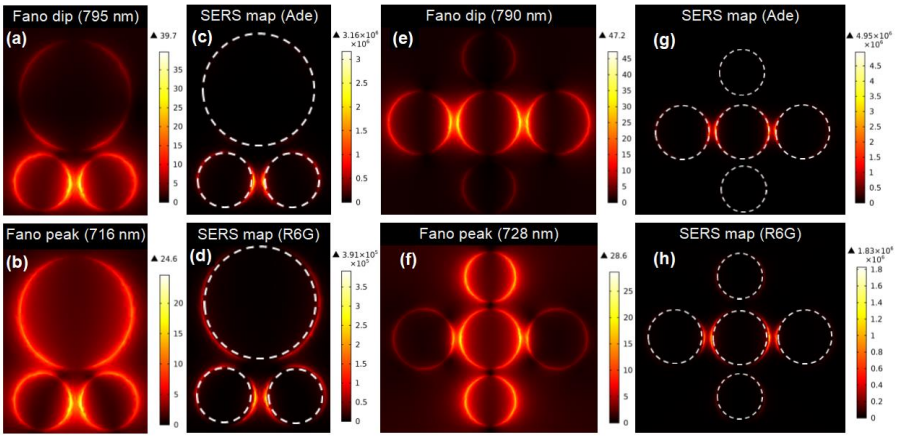

Fig. 3. Simulated NFE and SERS EEF maps calculated at a plane 1 nm above the top surface of the oligomers. (a-b) NFE plots for the trimer at Fano dip (795 nm) and Fano peak (716 nm). (c-d) SERS EEF maps of the trimer for the targeted Raman band of adenine (734 cm^{-1} or 833 nm) and rhodamine 6G (1360 cm^{-1} or 879 nm). (e-f) NFE plots for the pentamer at Fano dip (790 nm) and Fano peak (728 nm). (g-h) SERS EEF maps of the pentamer for the targeted Raman band of adenine (734 cm^{-1} or 833 nm) and rhodamine 6G (1360 cm^{-1} or 879 nm). In the plots (c-d) and (g-h), the white dashed lines represent the gold disks in the oligomer and for SERS EEF calculation, the excitation wavelength was considered as 785 nm. In (a-d) all the dimensions are along Fig. 1(a) and in (e-h) as illustrated in Fig. 1(b).

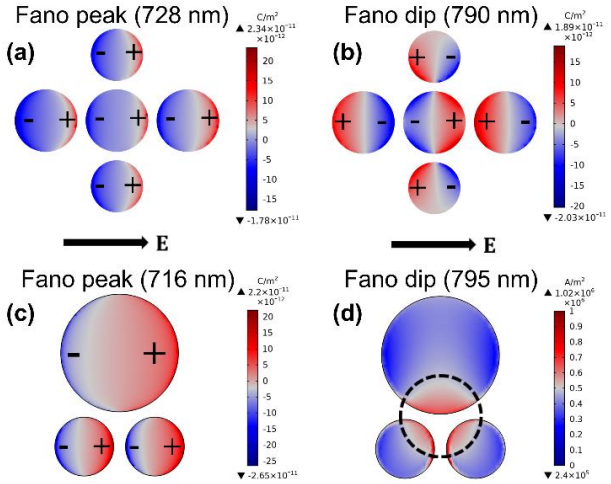

Fig. 4. Simulated surface charge densities and conduction current densities over the top surfaces of the disks present in the oligomers. (a-b) Surface charge density plots for the pentamer at Fano peak (728 nm) and Fano dip (790 nm). (c) Surface charge density plot for the trimer at Fano peak (716 nm). (d) Conduction current density plot for the trimer at Fano dip (795 nm). In the plots (a-d), the black arrows represent the polarization of the excitation electric field E.

The surface charge density plot for the trimer, depicted in Fig. 4(c), shows 'in-phase' plasmon oscillations in all disks at 716 nm and explains the creation of the broad super-radiant mode at that wavelength in corresponding scattering profile. The current density plot for the trimer at Fano dip (795 nm), illustrated in Fig. 4(d), reveals the presence of a 'coil type' magnetic resonant mode at 795 nm which has a sub-radiant nature in the scattering profile. Hence, the super-radiant mode in the trimer is electric in nature while the sub-radiant mode is magnetic (coil-type) and FR is originated from their hybridization [49-52].

Optics EXPRESS

The fabricated trimers and pentamers were arranged in a rectangular array with a gap of 2 μm between two adjacent oligomers to prevent direct crosstalk between them. The SEM images of the fabricated samples are presented in Fig. 5. Such oligomer arrays can be considered as periodic structures (reflective gratings) with a period of 2 μm and hence, they provide diffraction orders in their scattered light with scattering angle depending on wavelength. Of particular note is that in both fabricated structures, i.e. in the trimer and the pentamer (Fig. 5), the gaps between the bigger particles are slightly decreased due to the proximity effect in electron beam lithography. This effect was taken into account on the simulations also.

To determine the scattering intensity spectrum of the trimers and the pentamers, the first diffraction orders of the arrays were recorded at different angular positions, i.e., increment in the angle of detection redshifts the first diffraction order while its peak intensity follows the line shape of the scattering profile of an individual oligomer. To be specific, the intensity of the first diffraction order reached its minimum at an angle corresponding to the Fano dip, since, at that region, the nanostructures have a minimum in their scattering profile. Therefore, the peak intensities of the first diffraction order at different detection angles provide an intensity envelope from which the scattering profiles of the trimer and the pentamer can be extracted. The recorded peak intensities were normalized by dividing them with the lamp intensity at the corresponding spectral positions. The normalized intensities were further Lambertian corrected by dividing them with a cosine of the corresponding detection angle.

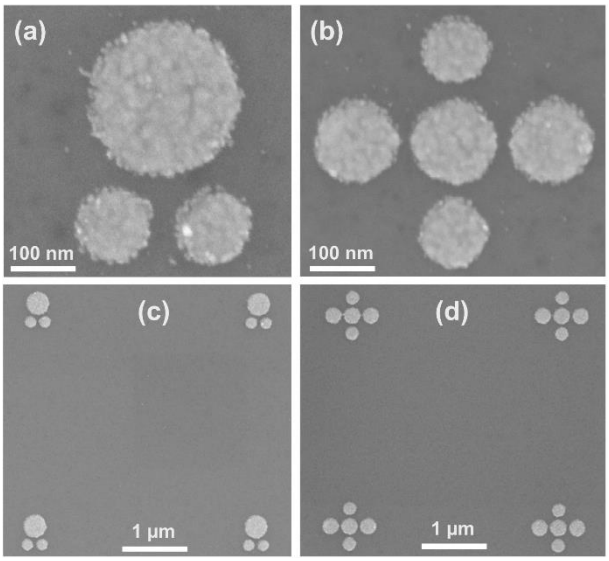

Fig. 5. SEM images of the fabricated oligomers. (a-b) SEM images of a single trimer and a single pentamer. (c-d) SEM images of the arrays of the trimer and the pentamer with 2 μm gap between two adjacent oligomers both in x and y direction.

Figure 6 shows the experimentally obtained scattering spectrum of the trimer and the pentamer along with their simulated estimations. The experimental spectra contain squares connected by dotted lines where the squares represent the measured peak intensities of the first diffraction order (normalized and Lambertian corrected) at different detection angles (and hence, at different spectral positions) thus forming the scattering intensity profiles of the oligomers. The experimental scattering profiles of the oligomers are in a good agreement with the simulated estimations and the pentamer shows stronger FR by yielding a lower value of k (k=0.25) than that of the trimer (k=0.46) in the experimental spectra.

Optics EXPRESS

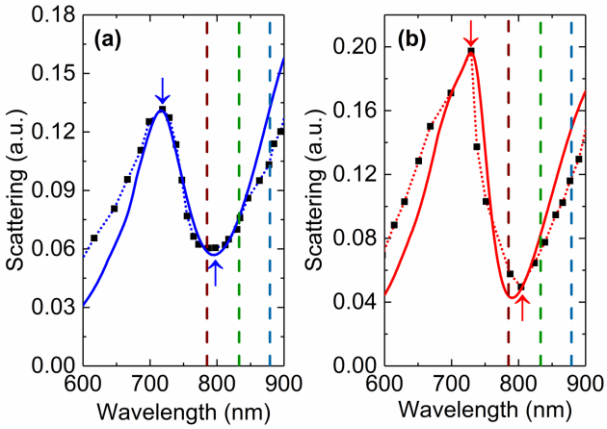

Fig. 6. (a) Simulated (solid blue line) scattering cross-section and experimental (dotted blue line) scattering intensity profiles of the trimer. (b) Simulated (solid red line) scattering cross-section and experimental (dotted red line) scattering intensity profiles of the pentamer. The simulated spectra are scaled with the experimental ones. The black squares in the experimental spectra represent the peak intensities of the first diffraction order (normalized and Lambertian corrected) collected at different detection angles. The red and blue arrows represent the position of the peak and the dip in the corresponding spectra used to calculate k. The red, green and blue (vertical) dashed lines in both diagrams represent, the excitation wavelength (785 nm), the targeted Raman line of adenine (734 cm^{-1} or 833 nm) and the targeted Raman line of rhodamine 6G (1360 cm^{-1} or 879 nm), respectively. For comparison between experimental scattering intensities of the trimer and the pentamer, please find Fig. 8 in Appendix.

To study the effect of FR on the SERS performance of the oligomers, we performed Raman spectroscopy of two Raman active analytes, adenine (Ade) and rhodamine 6G (R6G), on top of the trimers and the pentamers with an excitation at 785 nm. Our targeted Raman bands were the symmetric ring-breathing mode of adenine [54] around 734 cm^{-1} and C – C stretching mode (vibrational) of rhodamine 6G [53] around 1360 cm^{-1}. Collected SERS spectra were baseline-corrected using the asymmetric least squares algorithm for the baseline analysis [60] and smoothed using the Savitzky–Golay smoothing technique [61,62], both implemented by a commercially available data analysis software OriginPro 2017 [63]. The main areas of interest in Raman shifts were 1300 – 1400 cm^{-1} for R6G and 700 – 800 cm^{-1} for Ade during the collection. The resulting SERS spectra are presented in Fig. 7 and they are consistent with the existing literature [53,54,64-67]. The SERS spectrum of R6G shows also the N – H in-plane bend mode around 1312 cm^{-1} in addition to the targeted C – C vibrational stretching at 1363 cm^{-1}. No Raman signal was observed with the same amount of molecule, but without the oligomers.

Clearly, from Fig. 7, we can conclude that the pentamer, which has stronger FR in its simulated and experimental scattering profiles (in terms of the depth of the Fano dip, i.e., lower value of k) than the trimer, yielded stronger SERS signal than that of the trimer under the identical experimental conditions for both analytes. The obtained relative increases in the intensities of the targeted Raman lines were about 130% and even 330% for R6G and Ade, respectively. It should be noted that even the surface area of the pentamer is about 65% higher than that of the trimer, it would only account for a 65% increase in the SERS signal, when assuming constant surface concentration of the molecules, which is a reasonable assumption here. This is clearly not enough to explain the observed effect. In addition, the SERS signal of Ade is clearly higher than that of R6G, which could be due to the better matching of the FR to the targeted Raman line, but since the experimental conditions between different molecules differ, no proper conclusion can be drawn from that. Yet, the relative increase in the Raman line intensity when comparing the pentamer to the trimer is significantly higher for Ade, which can be addressed to the fact that the Raman line of Ade matches with the Fano-resonance, while

Optics EXPRESS

R6G Raman lines lie off from the resonance. The fact that the difference in SERS enhancement between the oligomers is higher for the Raman lines at FR than for the lines outside the resonance, implies that it is indeed the subradiant Fano mode that induces the highest SERS enhancement.

In this study, we did not focus to quantify explicitly any SERS enhancement factor for the trimer and the pentamer. However, since the detection sensitivity and number of molecules were same for one type of molecule and only the underlying nanostructure was changed, the induced increase in the SERS signal directly reflects the relative increase in the enhancement factor due to the oligomer properties. Thus, the above-mentioned experimental outcomes clearly present how the strength of FR directly influences the SERS activity of a plasmonic oligomer. Therefore, by engineering the strength of FR with a higher depth of Fano dip (or lower value of k) and by spectral tuning of FR at the targeted Raman region of the analytes as well as at the excitation wavelength, one can achieve higher SERS performance from a plasmonic oligomer.

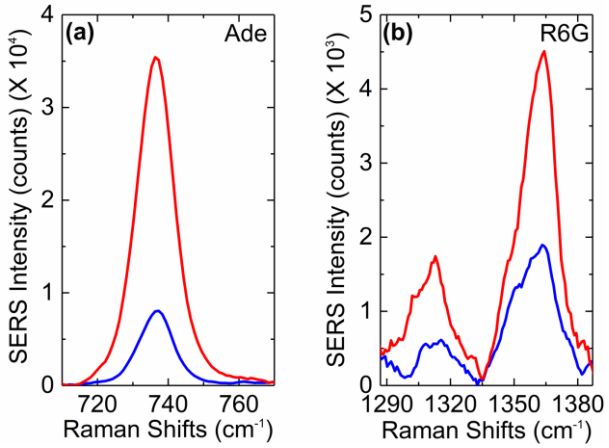

Fig. 7. (a) SERS intensity spectrum of the targeted Raman line of adenine (734 cm^{-1}) with the presence of the trimer (blue line) and the pentamer (red line). (b) SERS intensity spectrum of the targeted Raman lines of rhodamine 6G (1310 cm^{-1} and 1360 cm^{-1}) with the presence of the trimer (blue line) and the pentamer (red line). For complete spectra, please find Fig. 9 in Appendix.

4. Conclusions

Concisely, we designed and optimized two Fano-plasmonic disk-type gold oligomers using FEM-based simulations to ensure that their FR will overlap with our intended Raman lines of the analytes (1360 cm^{-1} for R6G and 734 cm^{-1} for adenine) recorded with the excitation wavelength of 785 nm. The simulated scattering profiles and the experimental scattering intensities of the fabricated oligomers clearly showed stronger FR (in terms of the depth of the Fano dip) in the pentamer than the trimer. The NFE plots and SERS maps of the oligomers also revealed that we achieved the spatial overlap of hotspots at the excitation and Raman wavelengths of the analytes. Our numerical analysis also explained that the origin of FR in the pentamer is electric in nature but in the trimer, FR originated from the interplay between the electric and the magnetic plasmon modes.

We then studied the SERS activity of the two oligomers having different strength and origin of FR. Our Raman analysis of the analytes resulted in higher enhancement of the Raman signal with the presence of the pentamer than that in the case of the trimer for both analytes. Consequently, from our experimental outcomes, we can conclude that the strength of FR in a Fano-plasmonic oligomer as well as its spectral overlap with the intended Raman lines significantly influences its SERS performance. Therefore, by suitable engineering of Fano lineshape, with stronger FR and spectral tuning with the intended Raman bands as well as with

Optics EXPRESS

the excitation frequency, one can achieve efficient SERS active substrates with spatially localized hotspots. We also got a hint that the optical properties and SERS activities of such oligomers may differ if their origin of FR differ but further studies required in this case to draw any concrete conclusions.

Appendix

Comparison between experimental scattering intensities of the trimer and the pentamer and complete SERS spectra of analytes.

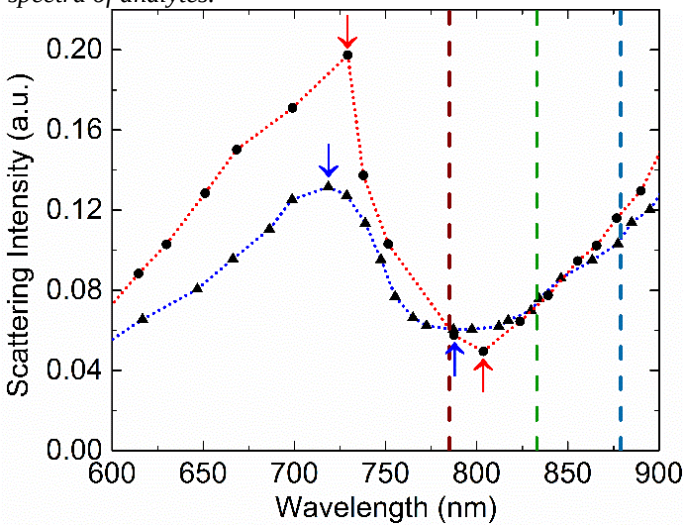

Fig. 8. Experimental scattering intensity profiles of the trimer (blue dotted line) and the pentamer (red dotted line). The black circles (in the red dotted line) and the black triangles (in the blue dotted line) represent the peak intensities of the first diffraction order (normalized and Lambertian corrected) collected at different detection angles. The red and blue arrows represent the position of the peak and the dip in the corresponding spectra used to calculate k. The red, green and blue (vertical) dashed lines represent, the excitation wavelength (785 nm), the targeted Raman line of adenine (734 cm^{-1} or 833 nm), and the targeted Raman line of rhodamine 6G (1360 cm^{-1} or 879 nm), respectively.

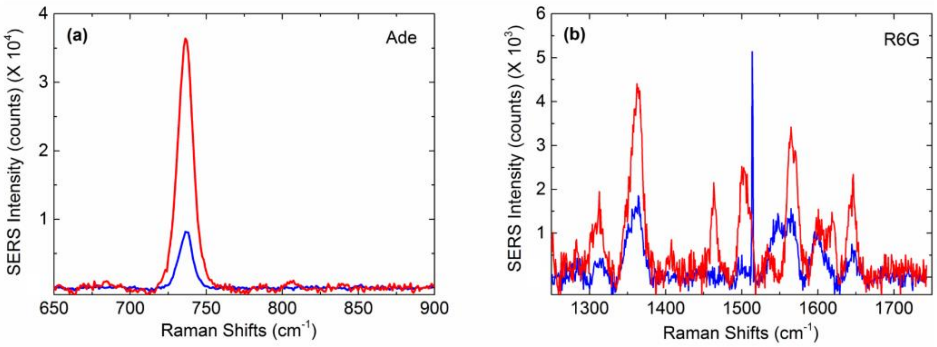

Fig. 9. (a) Complete SERS intensity spectrum of adenine (Ade) with the presence of the trimer (blue line) and the pentamer (red line). (b) Complete SERS intensity spectrum of rhodamine 6G (R6G) with the presence of the trimer (blue line) and the pentamer (red line). In (a-b), SERS spectra are reported without smoothing and baseline correction.

Funding

Academy of Finland (289947, 321066, 323995).

Optics EXPRESS

Acknowledgments

The authors gratefully acknowledge Prof. Kai-Erik Peiponen (University of Eastern Finland) and Prof. Mika Pettersson (University of Jyväskylä) for their valuable guidance during the research work, and Academy of Finland for funding.

Disclosures

The authors declare that there are no conflicts of interest related to this article.

References

1. D. Long, "Early history of the Raman effect," Int. Rev. Phys. Chem. **7** (4), 317-349 (1988).
2. C. Banwell, *Fundamentals of Molecular Spectroscopy* (McGraw-Hill, 1972), Chap. 4.
3. D. Long, *The Raman Effect: A Unified Treatment of The Theory of Raman Scattering by Molecules* (John Wiley & Sons, 2002).
4. D. Shipp, F. Sinjab, and I. Notingher, "Raman spectroscopy: techniques and applications in the life sciences," Adv. Opt. Photonics **9** (2), 315-428 (2017).
5. R. Das and Y. Agrawal, "Raman spectroscopy: recent advancements, techniques and applications," Vib. Spectrosc. **57**, 163-176 (2011).
6. C. Haynes, A. McFarland, and R. Van Duyne, "Surface-enhanced Raman spectroscopy," Anal. Chem. **77** (17), 338A-346A (2005).
7. M. Fleischmann, P. Hendra, and A. McQuillan, "Raman spectra of pyridine adsorbed at a silver electrode," Chem. Phys. Lett. **26**, 163-166 (1974).
8. S. Schlücker, "Surface-enhanced Raman spectroscopy: concepts and chemical applications," Angew. Chem. Int. Ed. **53**, 4756-4795 (2014).
9. B. Sharma, R. Frontiera, A. Henry, E. Ringe, and R. Van Duyne, "SERS: materials, applications, and the future," Mater. Today **15** (1-2), 16-25 (2012).
10. G. Schatz and R. Van Duyne, "Electromagnetic mechanism of surface-enhanced spectroscopy," in Surface-Enhanced Vibrational Spectroscopy, Handbook of Vibrational Spectroscopy vol. 1, J. Chalmers and P. Griffiths, eds. (John Wiley & Sons, 2002).
11. S. Ding, E. You, Z. Tian, and M. Moskovits, "Electromagnetic theories of surface-enhanced Raman spectroscopy," Chem. Soc. Rev. **46**, 4042-4076 (2017).
12. D. Cialla-May, X. Zheng, K. Weber, and J. Popp, "Recent progress in surface-enhanced Raman spectroscopy for biological and biomedical applications: from cells to clinics," Chem. Soc. Rev. **46**, 3945-3961 (2017).
13. C. Muehlethaler, M. Leona, and J. Lombardi, "Review of surface enhanced Raman scattering applications in forensic science," Anal. Chem. **88**, 152-169 (2016).
14. D. Chulhai, Z. Hu, J. Moore, X. Chen, and L. Jensen, "Theory of linear and nonlinear surface-enhanced vibrational spectroscopies," Annu. Rev. Phys. Chem. **67**, 541-564 (2016).
15. A. Henry, B. Sharma, M. Cardinal, D. Kurouski, and R. Van Duyne, "Surface-enhanced Raman spectroscopy biosensing: in vivo diagnostics and multimodal imaging," Anal. Chem. **88**, 6638-6647 (2016).
16. R. Tripp, R. Dluhy, and Y. Zhao, "Novel nanostructures for SERS biosensing," Nano Today **3** (3-4), 31-37 (2008).
17. K. Bantz, A. Meyer, N. Wittenberg, H. Im, Ö. Kurtulus, S. Lee, N. Lindquist, S-H. Oh, and C. Haynes, "Recent progress in SERS biosensing," Phys. Chem. Chem. Phys. **13**, 11551-11567 (2011).
18. E. Ru and P. Etchegoin, "Single-molecule surface-enhanced Raman spectroscopy," Annu. Rev. Phys. Chem. **63**, 65-87 (2012).
19. Y. Wang and J. Irudayaraj, "Surface-enhanced Raman spectroscopy at single-molecule scale and its implications in biology," Phil. Trans. R Soc. B **368**:20120026, 1-10 (2013).
20. H. Lee, S. Jin, H. Kim, and Y. Suh, "Single-molecule surface-enhanced Raman spectroscopy: a perspective on the current status," Phys. Chem. Chem. Phys. **15**, 5276-5287 (2013).
21. A. Zrimsek, N. Chiang, M. Mattei, S. Zaleski, M. McAnally, C. Chapman, A-I. Henry, G. Schatz, and R. Van Duyne, "Single-molecule chemistry with surface- and tip-enhanced Raman spectroscopy," Chem. Rev. **117**, 7583-7613 (2017).
22. J. Ye, F. Wen, H. Sobhani, J. Lassiter, P. Dorpe, P. Nordlander, and N. J. Halas, "Plasmonic nanoclusters: near-field properties of the Fano resonance interrogated with SERS," Nano Lett. **12** (3), 1660-1667 (2012).
23. M. Rahmani, B. Luk'yanchuk, and M. Hong, "Fano resonance in novel plasmonic nanostructures," Laser Photonics Rev. **7** (3), 329-349 (2013).
24. U. Fano, "On the absorption spectrum of noble gases at the arc spectrum limit," Nuovo Cimento **12**, 154-161 (1935).
25. B. Luk'yanchuk, N. Zheludev, S. Maier, N. J. Halas, P. Nordlander, H. Giessen, and C. Chong, "The Fano resonance in plasmonic nanostructures and metamaterials," Nat. Mater. **9**, 707-715 (2010).
26. A. Miroshnichenko, S. Flach, and Y. Kivshar, "Fano resonances in nanoscale structures," Rev. Mod. Phys. **82**, 2257-2298 (2010).

Optics EXPRESS

27. M. Limonov, M. Rybin, A. Poddubny, and Y. Kivshar, "Fano resonances in photonics," Nat. Photon. **11**, 543-554 (2017).
28. U. Fano, "Effects of configuration interaction on intensities and phase shifts," Phys. Rev. **124**, 1866-1878 (1961).
29. S. Emami, R. Penny, H. Rashid, W. Mohammed, and B. Rahman, "Fano resonance in plasmonic optical antennas," in Reviews in Plasmonics 2015, C. Geddes, ed. (Springer, 2016).
30. M. Hentschel, D. Dregely, R. Vogelgesang, H. Giessen, and N. Liu, "Plasmonic oligomers: the role of individual particles in collective behavior," ACS Nano **5** (3), 2042-2050 (2011).
31. M. Hentschel, M. Saliba, R. Vogelgesang, H. Giessen, P. Alivisatos, and N. Liu, "Transition from isolated to collective modes in plasmonic oligomers," Nano Lett. **10** (7), 2721-2726 (2010).
32. Y. Zhang, F. Wen, Y-R. Zhen, P. Nordlander, and N. J. Halas, "Coherent Fano resonances in a plasmonic nanocluster enhance optical four-wave mixing," Proc. Natl. Acad. Sci. U.S.A. **110** (23), 9215-9219 (2013).
33. J. Fan, K. Bao, C. Wu, J. Bao, R. Bardhan, N. J. Halas, V. Manoharan, G. Shvets, P. Nordlander, and F. Capasso, "Fano-like interference in self-assembled plasmonic quadrumer clusters," Nano Lett. **10** (11), 4680-4685 (2010).
34. B. Gallinet and O. Martin, "Influence of electromagnetic interactions on the line shape of plasmonic Fano resonances," ACS Nano **5** (11), 8999-9008 (2011).
35. B. Lassiter, H. Sobhani, M. Knight, W. Mielczarek, P. Nordlander, and N. J. Halas, "Designing and deconstructing the Fano lineshape in plasmonic nanoclusters," Nano Lett. **12**, 1058-1062 (2012).
36. S. Zhang, D. Genov, Y. Wang, M. Liu, and X. Zhang, "Plasmon-induced transparency in metamaterials," Phys. Rev. Lett. **101**, 0474011-0474014 (2008).
37. B. Lassiter, H. Sobhani, J. Fan, J. Kundu, F. Capasso, P. Nordlander, and N. J. Halas, "Fano resonances in plasmonic nanoclusters: geometrical and chemical tenability," Nano Lett. **10** (8), 3184-3189 (2010).
38. M. Rahmani, B. Lukiyanchuk, T. Tahmasebi, Y. Lin, T. Liew, and M. Hong, "Polarization-controlled spatial localization of near-field energy in planar symmetric coupled oligomers," Appl. Phys. A **107**, 23-30 (2012).
39. B. Gallinet and O. Martin, "Relation between near–field and far–field properties of plasmonic Fano resonances," Opt. Express **19** (22), 22167-22175 (2011).
40. Y. Joe, A. Satanin, and C. Kim, "Classical analogy of Fano resonances," Phys. Scr. **74**, 259-266 (2006).
41. A. Lovera, B. Gallinet, P. Nordlander, and O. Martin, "Mechanisms of Fano resonances in coupled plasmonic systems," ACS Nano **7** (5), 4527-4536 (2013).
42. M. Rahmani, T. Tahmasebi, Y. Lin, B. Lukiyanchuk, T. Liew, and M. Hong, "Influence of plasmon destructive interferences on optical properties of gold planar quadrumers," Nanotechnology **22**, 1-7 (2011).
43. M. Rahmani, D. Lei, V. Giannini, B. Lukiyanchuk, M. Ranjbar, T. Liew, M. Hong, and S. Maier, "Subgroup decomposition of plasmonic resonances in hybrid oligomers: modeling the resonance lineshape," Nano Lett. **12** (4), 2101-2106 (2012).
44. A. Attaran, S. Emami, M. Soltanian, R. Penny, F. Behbahani, S. Harun, H. Ahmad, H. Abdul-Rashid, and M. Moghavvemi, "Circuit model of Fano resonance on tetramers, pentamers and broken symmetry pentamers," Plasmonics **9**, 1303-1313 (2014).
45. B. Gallinet and O. Martin, "Ab-initio theory of Fano resonances in plasmonic nanostructures and metamaterials," Phys. Rev. B **83**, 2354271-2354276 (2011).
46. M. Rahmani, B. Lukiyanchuk, B. Ng, A. Tavakkoli, T. Liew, and M. Hong, "Generation of pronounced Fano resonances and tuning of subwavelength spatial light distribution in plasmonic pentamers," Opt. Express **19** (6), 4949-4956 (2011).
47. M. Rahmani, B. Lukiyanchuk, T. Nguyen, T. Tahmasebi, Y. Lin, T. Liew, and M. Hong, "Influence of symmetry breaking in pentamers on Fano resonance and near-field energy localization," Opt. Mater. Express **1** (8), 1409-1415 (2011).
48. Y. Zhang, Y. Zhen, O. Neumann, J. Day, P. Nordlander, and N. J. Halas, "Coherent anti-Stokes Raman scattering with single-molecule sensitivity using a plasmonic Fano resonance," Nat. Commun. **5**, 4424 (2014).
49. J. Wang, C. Fan, J. He, P. Ding, E. Liang, and Q. Xue, "Double Fano resonances due to interplay of electric and magnetic plasmon modes in planar plasmonic structure with high sensing sensitivity," Opt. Express **21** (2), 2236-2244 (2013).
50. S. Sheikholeslami, A. Etxarri, and J. Dionne, "Controlling the interplay of electric and magnetic modes via Fano-like plasmon resonances," Nano Lett. **11** (9), 3927-3934 (2011).
51. J. He, C. Fan, P. Ding, S. Zhu, and E. Liang, "Near-field engineering of Fano resonances in a plasmonic assembly for maximizing CARS enhancements," Sci. Rep. **6**, 20777 (2016).
52. A. Nazir, S. Panaro, R. Zaccaria, C. Liberale, F. Angelis, and A. Toma, "Fano coil-type resonance for magnetic hot-spot generation," Nano Lett. **14** (6), 3166-3171 (2014).
53. C. Wu, E. Chen, and J. Wei, "Surface enhanced Raman spectroscopy of rhodamine 6G on agglomerates of different-sized silver truncated nanotriangles," Colloids Surf. A: Physicochem. Eng. Aspects **506**, 450-456 (2016).
54. F. Madzharova, Z. Heiner, M. Gühlke, and J. Kneipp, "Surface-enhanced hyper-Raman spectra of adenine, guanine, cytosine, thymine and uracil," J. Phys. Chem. C 120, 15415-15423 (2016).
55. COMSOL Multiphysics application gallery, "Scatterer on substrate" (COMSOL Multiphysics, 2019). https://www.comsol.fi/model/download/563151/models.woptics.scatterer_on_substrate.pdf
56. P. Johnson and R. Christy, "Optical constants of the noble metals," Phys. Rev. B **6**, 4370-4379 (1972).

Optics EXPRESS

57. S. Baieva, O. Hakamaa, G. Groenhof, T. Heikkila, and J. J. Toppari, "Dynamics of strongly coupled modes between surface plasmon polaritons and photoactive molecules: the effect of the Stokes shift," ACS Photonics **4** (1), 28-37 (2017).
58. T. Hakala, J. J. Toppari, A. Kuzyk, M. Pettersson, H. Tikkanen, H. Kunttu, and P. Törmä, "Vacuum Rabi splitting and strong-coupling dynamics for surface-plasmon polaritons and rhodamine 6G molecules," Phys. Rev. Lett. **103**, 0536021-0536024 (2009).
59. M. Koponen, U. Hohenester, T. Hakala, and J. J. Toppari, "Absence of mutual polariton scattering for strongly coupled surface plasmon polaritons and dye molecules with a large Stokes shift," Phys. Rev. B: Condens. Matter Mater. Phys. **88**, 0854251-0854258 (2013).
60. S. He, W. Zhang, L. Liu, Y. Huang, J. He, W. Xie, P. Wu, and C. Du, "Baseline correction for Raman spectra using an improved asymmetric least squares method," Anal. Methods **6**, 4402-4407 (2014).
61. J. Luo, K. Ying, and J. Bai, "Savitzky–Golay smoothing and differentiation filter for even number data," Signal Processing **85**, 1429-1434 (2005).
62. M. Clupek, P. Matejka, and K. Volka, "Noise reduction in Raman spectra: finite impulse response filtration versus Savitzky–Golay smoothing," J. Raman Spectrosc. **38**, 1174-1179 (2007).
63. OriginLab documentation, "Origin user guide" (OriginLab, 2017). https://www.originlab.com/pdfs/Origin2017_Documentation/English/Origin_User_Guide_2017_E.pdf
64. J. Kundu, O. Neumann, B. Janesko, D. Zhang, S. Lal, A. Barhoumi, G. Scuseria, and N. J. Halas, "Adenine- and adenosine monophosphate (AMP)-gold binding interactions studied by surface-enhanced Raman and infrared spectroscopies," J. Phys. Chem. C **113**, 14390-14397 (2009).
65. K. Kneipp, R. Dasari, and Y. Wang, "Near-infrared surface-enhanced Raman scattering (NIR SERS) on colloidal silver and gold," Appl. Spectrosc. **48** (8), 951-955 (1994).
66. E. Kohr, B. Karawdeniya, J. Dwyer, A. Gupta, and W. Euler, "A comparison of SERS and MEF of rhodamine 6G on a gold substrate," Phys. Chem. Chem. Phys. **19**, 27074-27080 (2017).
67. M. Suzuki, Y. Niidome, Y. Kuwahara, N. Terasaki, K. Inoue, and S. Yamada, "Surface-enhanced nonresonance Raman scattering from size- and morphology-controlled gold nanoparticle films," J. Phys. Chem. B **108**, 11660-11665 (2004).

130.234.183.57 {ts '2019-10-03 07:13:34'}